

SURFACE WAVES EXTRACTION OF A CONDUCTIVE SHEET EMBEDDED IN A MULTILAYER ENVIRONMENT

*

In this chapter, we compute the dispersion diagrams of an infinitesimally thin conductive sheet that lies embedded in a stack of semiconductors. The possibility of wave propagation along the sheet is investigated by searching for poles of an equivalent transmission line Green function determined by the multilayer structure. A numerical root-finding routine is presented that permits complex-valued solutions and avoids singularities in the complex plane.

1 Theory

1.1 Derivation of Transmission line Green Function

We follow the well-established approach of field computation for planar multilayered media [1, 2], in which an equivalent transmission line network is set up for the structure. As shown in Fig. 3a, it is assumed that the structure is unbounded in the lateral direction.

*Last Modified: 02:06, Tuesday 23rd May, 2017.

The electric and magnetic fields are given by the Maxwell's equations,

$$\nabla \times \mathbf{E} = -j\omega\mu\mathbf{H}, \quad (1a)$$

$$\nabla \times \mathbf{H} = j\omega\epsilon\mathbf{E} + \mathbf{J}. \quad (1b)$$

For boundary-value problems displaying symmetry along the z direction, it is desirable to decompose the ∇ operator into two components, one d/dz and the other a transverse (to z) operator, ∇_t [3, p. 64]. By taking the Fourier transform,

$$\mathcal{F}[f(\mathbf{r})] \equiv \tilde{f}(\mathbf{k}_\rho, z) = \int_{-\infty}^{\infty} \int_{-\infty}^{\infty} f(\mathbf{r}) e^{-j\mathbf{k}_\rho \cdot \rho} dx dy \quad (2)$$

the field computation is simplified by switching to the spectral frequency domain \mathbf{k}_ρ , which reduces the vector differential operator, ∇ to $-jk_x\hat{\mathbf{x}} - jk_y\hat{\mathbf{y}} + d/dz\hat{\mathbf{z}}$. In (2), the cylindrical coordinates are expressed as,

$$\rho = x\hat{\mathbf{x}} + y\hat{\mathbf{y}}, \quad \text{and} \quad \mathbf{k}_\rho = k_x\hat{\mathbf{x}} + k_y\hat{\mathbf{y}}, \quad (3)$$

and the notation \sim above the terms indicates the Fourier transform with respect to the transverse coordinates and from here on, will be used to denote the spectral domain quantities.

As stated earlier, it is advantageous to separate the fields in transverse and longitudinal coordinates since, as we shall shortly see, the longitudinal part of the field can be completely expressed in terms of the transverse component. Applying the Fourier transform (2) on the Maxwell's equations (1), we obtain:

$$\left(-j\mathbf{k}_\rho + \hat{\mathbf{z}} \frac{d}{dz} \right) \times (\tilde{\mathbf{E}}_t + \tilde{\mathbf{E}}_z) = -j\omega\mu(\tilde{\mathbf{H}}_t + \tilde{\mathbf{H}}_z), \quad (4a)$$

$$\left(-j\mathbf{k}_\rho + \hat{\mathbf{z}} \frac{d}{dz} \right) \times (\tilde{\mathbf{H}}_t + \tilde{\mathbf{H}}_z) = j\omega\epsilon(\tilde{\mathbf{E}}_t + \tilde{\mathbf{E}}_z) - (\tilde{\mathbf{J}}_t + \tilde{\mathbf{J}}_z). \quad (4b)$$

The transverse and longitudinal components of the magnetic field can be separately expressed in (4a) as,

$$-j\mathbf{k}_\rho \times \tilde{\mathbf{E}}_z + \frac{d}{dz} \hat{\mathbf{z}} \times \tilde{\mathbf{E}}_t = -j\omega\mu\tilde{\mathbf{H}}_t, \quad (5a)$$

$$-j\mathbf{k}_\rho \times \tilde{\mathbf{E}}_t = -j\omega\mu\tilde{\mathbf{H}}_z. \quad (5b)$$

Using the vector cross product property [4, p. 117],

$$\mathbf{A} \times \mathbf{B} = \mathbf{A} \cdot (\mathbf{B} \times \hat{\mathbf{n}}) \hat{\mathbf{n}}, \quad (6)$$

where the unit vector $\hat{\mathbf{n}}$ is normal to the plane containing vectors \mathbf{A} and \mathbf{B} . A scalar form of the longitudinal component of the electric field is obtained by applying (6) on (5b),

$$-j\mathbf{k}_\rho \cdot (\tilde{\mathbf{E}}_t \times \hat{\mathbf{z}}) \hat{\mathbf{z}} = -j\omega\mu\tilde{\mathbf{H}}_z \quad (7)$$

which can be written in the scalar form,

$$-j\tilde{H}_z = \frac{-j}{\omega\mu} \mathbf{k}_\rho \cdot (\tilde{\mathbf{E}}_t \times \hat{\mathbf{z}}). \quad (8)$$

Now taking the vector product with unit vector $\hat{\mathbf{z}}$ on both sides of (5a), the transverse electric field component is expressed as:

$$\begin{aligned} \frac{d\tilde{\mathbf{E}}_t}{dz} &= -j(\mathbf{k}_\rho \times \tilde{\mathbf{E}}_z) \times \hat{\mathbf{z}} - j\omega\mu\tilde{\mathbf{H}}_t \times \hat{\mathbf{z}} \\ &= -j\mathbf{k}_\rho \tilde{E}_z - j\omega\mu\tilde{\mathbf{H}}_t \times \hat{\mathbf{z}} \end{aligned} \quad (9)$$

where the BAC-CAB vector triple product identity, $(\mathbf{A} \times \mathbf{B}) \times \mathbf{C} \equiv \mathbf{B}(\mathbf{A} \cdot \mathbf{C}) - \mathbf{C}(\mathbf{A} \cdot \mathbf{B})$ has been applied.

Following a similar procedure starting from (4b), we obtain the transverse component of magnetic field, along with the scalar longitudinal component of electric field:

$$\begin{aligned} \frac{d\tilde{\mathbf{H}}_t}{dz} &= -j(\mathbf{k}_\rho \times \tilde{\mathbf{H}}_z) \times \hat{\mathbf{z}} + j\omega\epsilon\tilde{\mathbf{E}}_t \times \hat{\mathbf{z}} + \tilde{\mathbf{J}}_t \times \hat{\mathbf{z}} \\ &= -j\mathbf{k}_\rho \tilde{H}_z + j\omega\epsilon\tilde{\mathbf{E}}_t \times \hat{\mathbf{z}} + \tilde{\mathbf{J}}_t \times \hat{\mathbf{z}}, \end{aligned} \quad (10)$$

and,

$$-j\omega\epsilon\tilde{E}_z = j\mathbf{k}_\rho \cdot (\tilde{\mathbf{H}}_t \times \hat{\mathbf{z}}) + \tilde{J}_z. \quad (11)$$

By substituting (11) in (9), we get the transverse component of electric field,

$$\frac{d\tilde{\mathbf{E}}_t}{dz} = \frac{1}{j\omega\epsilon} \left(k^2 - \mathbf{k}_\rho \mathbf{k}_\rho \cdot \right) (\tilde{\mathbf{H}}_t \times \hat{\mathbf{z}}) + \mathbf{k}_\rho \frac{\tilde{J}_z}{\omega\epsilon}. \quad (12)$$

Similarly, from (8) and (10), the transverse component of magnetic field,

$$\frac{d\tilde{\mathbf{H}}_t}{dz} = \frac{1}{j\omega\mu} \left(k^2 - \mathbf{k}_\rho \mathbf{k}_\rho \cdot \right) (\hat{\mathbf{z}} \times \tilde{\mathbf{E}}_t) + \tilde{\mathbf{J}}_t \times \hat{\mathbf{z}} \quad (13)$$

where $k = \omega\sqrt{\mu\epsilon}$ in (12) and (13) is the medium wavenumber.

The fields in (12) and (13) for arbitrarily aligned sources lie in the plane of a spectral

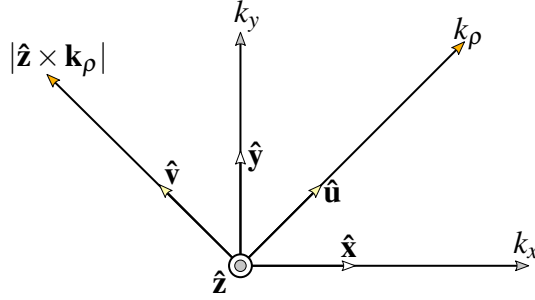


Figure 1: Coordinate System transformation in the spectral domain

coordinate system as illustrated in Fig. 1. A rotational transformation of the coordinate system such that the axes align with the vectors $\mathbf{k}_\rho, \hat{\mathbf{z}} \times \mathbf{k}_\rho$ [5], simplifies the procedure of finding the transmission line equivalent, which allows the TE and TM mode analysis to be made separately. The coordinate transformation can be expressed as:

$$\begin{bmatrix} \hat{\mathbf{u}} \\ \hat{\mathbf{v}} \end{bmatrix} = \begin{bmatrix} \cos \phi & \sin \phi \\ -\sin \phi & \cos \phi \end{bmatrix} \begin{bmatrix} \hat{\mathbf{x}} \\ \hat{\mathbf{y}} \end{bmatrix} \quad (14)$$

where ϕ is the angle between \mathbf{k}_ρ and the positive x-axis. A transmission line analogue for the spectral fields, expressed in terms of modal voltages and currents can therefore, be written as [6, 1],

$$\begin{bmatrix} \tilde{\mathbf{E}}_t \\ \tilde{\mathbf{H}}_t \end{bmatrix} = \begin{bmatrix} V^{TM} & V^{TE} \\ -I^{TE} & I^{TM} \end{bmatrix} \begin{bmatrix} \hat{\mathbf{u}} \\ \hat{\mathbf{v}} \end{bmatrix}. \quad (15)$$

Using the results of (15) in (12) and noting that $\hat{\mathbf{u}} = \mathbf{k}_\rho / k_\rho$, we get,

$$\frac{d(\hat{\mathbf{u}}V^{TM} + \hat{\mathbf{v}}V^{TE})}{dz} = \frac{1}{j\omega\epsilon} (\mathbf{k}_\rho \cdot \mathbf{k}_\rho) (\hat{\mathbf{u}}I^{TM} + \hat{\mathbf{v}}I^{TE}) + \hat{\mathbf{u}} \frac{k_\rho}{\omega\epsilon} \tilde{J}_z \quad (16)$$

By separating the $\hat{\mathbf{u}}$ and $\hat{\mathbf{v}}$ components, we obtain the TM and TE equivalent voltage equations respectively,

$$\frac{dV^{TM}}{dz} = \frac{1}{j\omega\epsilon} (k^2 - k_\rho^2) I^{TM} + \frac{k_\rho}{\omega\epsilon} \tilde{J}_z, \quad (17a)$$

$$\frac{dV^{TE}}{dz} = \frac{k^2}{j\omega\epsilon} I^{TE}. \quad (17b)$$

Similarly, from (15) and (13), the equivalent current equations can be written as:

$$\frac{dI^{TM}}{dz} = \frac{k^2}{j\omega\mu} V^{TM} - \tilde{J}_u, \quad (18a)$$

$$\frac{dI^{TE}}{dz} = \frac{-1}{j\omega\mu} (k^2 - k_\rho^2) V^{TE} + \tilde{J}_v. \quad (18b)$$

Equations (17)-(18) can be conveniently written in a compact form as a set of Telegrapher's equations [2, p. 1166]:

$$\frac{dV^\alpha}{dz} = -jk_z Z^\alpha I^\alpha + v^\alpha \quad (19a)$$

$$\frac{dI^\alpha}{dz} = -jk_z Y^\alpha V^\alpha + i^\alpha \quad (19b)$$

where the propagation constant in the transverse direction is,

$$k_z = \pm \sqrt{k^2 - k_\rho^2} \quad (20)$$

and the modal impedances are,

$$Z^{TM} = \frac{1}{Y^{TM}} = \frac{k_z}{\omega\epsilon}, \quad (21a)$$

$$Z^{TE} = \frac{1}{Y^{TE}} = \frac{\omega\mu}{k_z}. \quad (21b)$$

Assuming only electric sources existing in space, the corresponding TL sources, v^α and i^α , where α is either TE or TM, are illustrated in 2. A horizontally oriented (x-directed) electric dipole is represented by a current source in an equivalent TM transmission line network. Likewise, the equivalent configuration of a vertical (y-directed) electric dipole is a TE network with a current source. A z-directed dipole corresponds to voltage source in a TM transmission line. For an arbitrarily directed source, the equivalent TL model consists of a superposition of the three representations.

1.2 Equivalent TL network of semiconductor heterostructures

In modern semiconductor devices such as a field-effect transistor, multiple layers of materials with slightly different dielectric properties and band-gap energies are epitaxially grown over each other. Of particular interest are the group III-V materials in which extraordinary electromagnetic interfacial phenomena is observed, mainly due to formation of

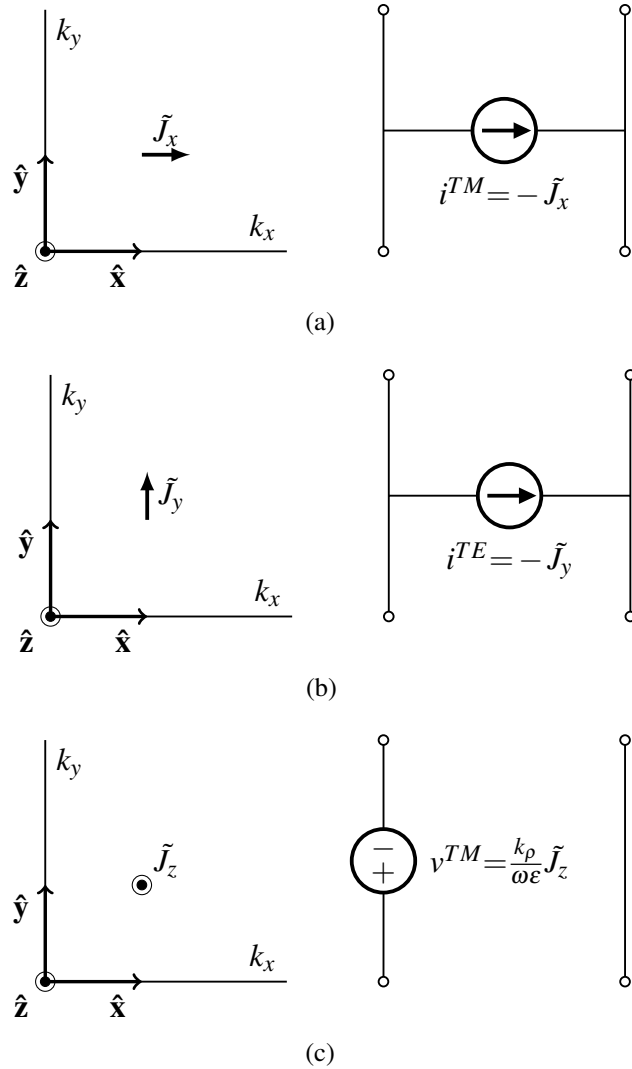


Figure 2: Electric Source representation in a transmission line network

a two-dimensional electron gas (2DEG) at the interface. To develop an understanding of the unusual properties of what are commonly called semiconductor heterostructures, we construct an equivalent transmission model of the layered structure using the theory discussed in the previous section.

An illustration of a multilayer setup with a heterostructure near the top of the transistor substrate, through which modern devices like the high electron mobility transistor operate, is shown in Fig. 3a. Although a number of other material layers lie underneath the heterostructure that are essential to the fabrication process, primarily to strengthen the

epitaxial structure, only the top layers are conducive to an electric field. Moreover, since the widths of the layers in the heterostructure are much smaller than the rest of the layers in the substrate stack, we assume that the heterostructure is unbounded from the bottom.

The 2DEG which is only a few atoms wide in thickness, is a highly conductive region with an abundance of free electrons, which can be expressed in terms of a surface conductivity [7],

$$\sigma_s = \frac{N_s e^2 \tau}{m^*} \frac{1}{1 + j\omega\tau}, \quad (22)$$

where N_s is the free electron concentration at the interface, e is the electron charge, m^* is the effective electron mass in the heterostructure, τ is the scattering time of electrons, and ω is the angular frequency. For a wave propagating along the interface, the electron scattering time which is highly temperature dependent, determines the attenuation factor. At room temperature, the thermal vibrations of electrons result in a very small value of τ which is of the order of femtoseconds (1×10^{-15} s), leading to a high-loss scenario. On the other hand, when the heterostructure is cooled to temperatures close to the boiling point of helium (4.2 K), thermal vibrations are effectively removed and the losses are consequently minimized.

In a transmission line analogue, the equivalent representation of a conductive sheet such as a 2DEG is a shunt admittance as shown in Fig. 3b. In a high electron mobility transistor, when a voltage bias is applied across the source and drain terminals, a current starts to flow laterally, inside the 2DEG. Such a current source, configured horizontally corresponds to Fig. 2a, which translates to a TM-mode transmission line excited by a current source. The presence of a gate terminal above or below the interface allows the electron concentration to be modified by the gate voltage. Therefore, instead of an independent current source in the equivalent transmission line network, a voltage-controlled current source is placed as indicated in Fig. 3.

We determine the dispersion relation in a 2DEG region which lies embedded in a semiconductor stack. As stated earlier, the active state of the transistor in which a current flows through the 2DEG corresponds to a TM-mode transmission line network. It must

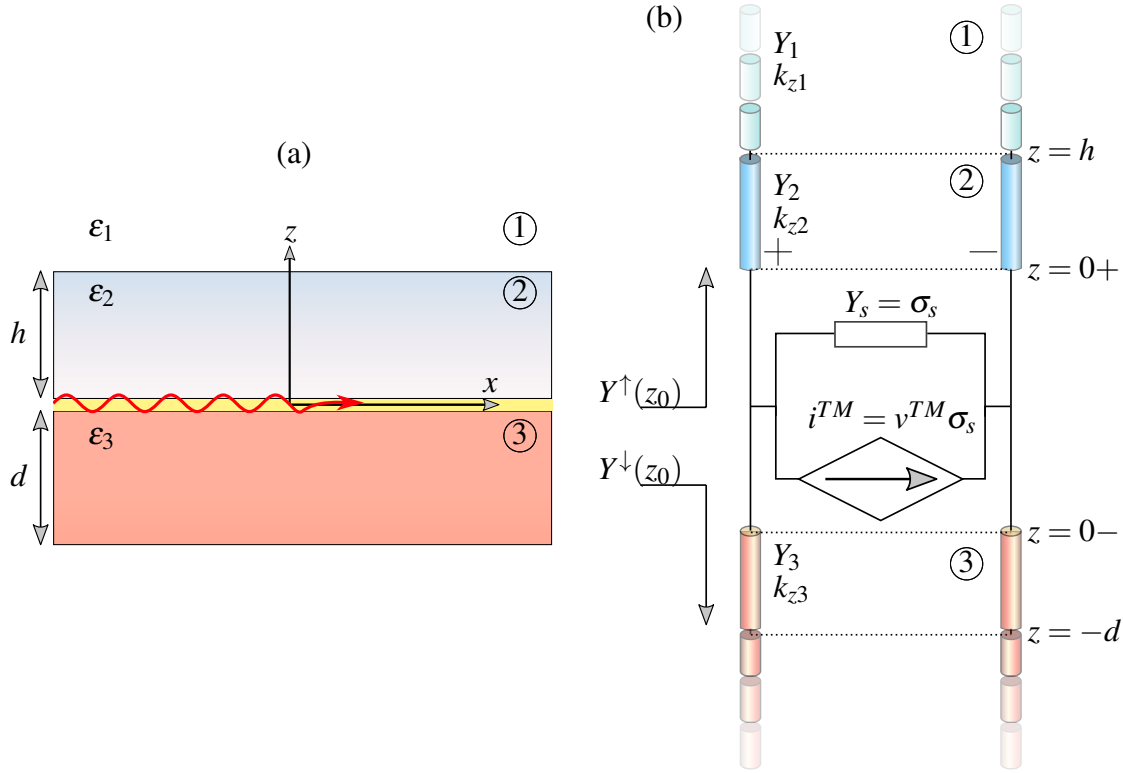


Figure 3: (a) Multilayer structure typically found in a high electron mobility transistor, (b) Equivalent transmission line network

also be mentioned that a similar TL analogue can be obtained if the physical structure is excited by a TM-polarized plane wave. The dispersion relation can be written using the transverse resonance method that requires the total admittance as seen from the 2DEG (at $z = 0$) to be zero [8],

$$Y^\uparrow(z_0) + Y^\downarrow(z_0) + Y_\sigma = 0. \quad (23)$$

Here, $Y^\uparrow(z_0)$ and $Y^\downarrow(z_0)$ are the up- and down-looking TL admittances from the 2DEG located at $z = 0$ and $Y_\sigma = \sigma_s$ from (22).

A nontrivial solution of (23) in terms of the propagation constant k_ρ yields the surface wave modes of the structure in the complex k-plane.

2 Surface waves extraction technique

We seek to solve (24) in the complex z-plane to obtain the zeros, z_k in a given search region \mathbb{C} . For a multilayer problem such as the one shown in Fig. 3a, f represents the dispersion relation (23) which, in fact is the denominator of the transmission line Green function (TLGF). From hereon, k_ρ is replaced by z for notational simplicity. Depending on the location of the zeros of the function f in the complex plane, z_k 's can be termed as the surface wave modes of the multilayer or synonymously, poles of the TLGF.

$$f(k_\rho) = 0 \quad (24)$$

Although the problem at first, may appear to be a relatively simple root-search in which readily available and popular iterative algorithms like the Newton or Halley's method can be applied, complication arises due to the presence of complex-valued roots. Furthermore, the convergence of the aforementioned methods is highly subject to an initial guess that must lie close to the actual root. As an example, basins of attraction, which illustrate the convergence rate of an initial guess, are shown in Fig. 4 for Newton's and Halley's methods which are two of the most popular iterative root-finding methods. In Fig. 4, the actual roots of a polynomial, $z^{10} - 1$ are depicted by circle marks. The regions are color-coded for each root where a large area of a particular color indicates that if the initial guess is located in that region, convergence to the respective root will be achieved quickly. On the other hand, if the initial guess lies in the fractal region, the convergence is very slow. Another observation through which Newton and Halley's methods can be compared is that the basins of attraction of Newton's method, shown in Fig. 4a have a denser fractal region due to its quadratic complexity of convergence. On the contrary, the Halley's method, which is cubic, the fractals are comparatively sparse as shown in Fig. 4b.

For a dispersion relation (23), which is defined by a transcendental equation, presence of singularities, particularly in the vicinity of an actual solution may leave an iterative method completely divergent or yet churn out a bogus and unreliable answer.

Argument principle method (APM) is a robust, complex root-finding algorithm in which

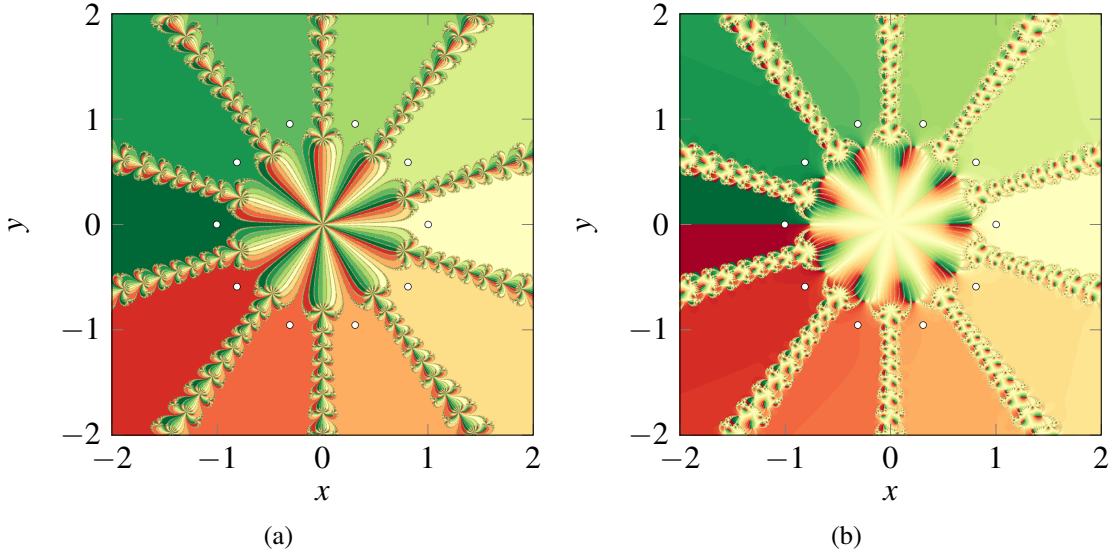


Figure 4: Complex plane basin of attraction while solving $z^{10} - 1 = 0$ using: (a) Newton's method (c) Halley's method

convergence is guaranteed within a specified region without supplying any initial guess [9, 10, 11, 12, 13, 14, 15]. It requires the function to be analytic in the specified search region. A pictorial representation of this technique is shown in Fig. 5 where the roots inside a specified region Γ in the complex plane are computed by approximating the given function with a polynomial. In case, the number of zeros inside Γ exceed a pre-allocated value N_r , the search region is subdivided into smaller regions. Moreover, the function f must be non-zero at the boundary of Γ . The following sections briefly describe each step of the method.

2.1 Counting the zeros

To develop an efficient method of locating the zeros, we assume that the function f is analytic, which implies that it is differentiable and free from any singularities. It is also required that f is non-zero at the boundary, Γ of the region \mathbb{C} . The search region is set as rectangular, mainly because of ease in programming it. The number of zeros, N inside a

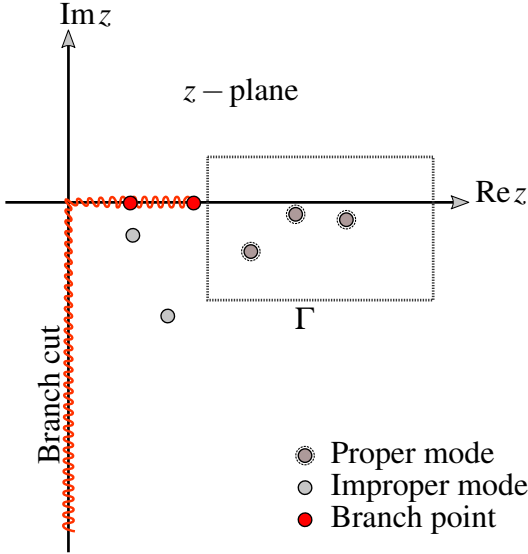


Figure 5: Illustration of the root-finding routine in the presence of branch point singularities. Only proper modes are sought within a rectangular contour Γ

region with a boundary Γ can be found using the Cauchy's integral theorem [16, 9, pg. 71],

$$N = \frac{1}{2\pi j} \oint_{\Gamma} \frac{f'(z)}{f(z)} dz \quad (25)$$

where the integrand is a logarithmic derivative of the function. The analytical derivative of functions such as found in dispersion relations like (23) are seldom readily-available and it is generally cumbersome to compute. In this chapter, we use approximate the derivative by a finite difference formula,

$$f'(z) = \frac{f(z+h) - f(z-h)}{2h}, \quad (26)$$

where $h \sim \sqrt{\varepsilon_m}$ and $\varepsilon_m = 2.220 \times 10^{-16}$ is the double-precision machine accuracy [17, pg. 230].

In addition to (25), a derivative-free form of the argument principle [10, 14], which may be preferred in certain cases is,

$$N = \frac{1}{2\pi} \oint_{\Gamma} d\{\arg f(k_\rho)\}, \quad (27)$$

The value of both the integrals, i.e., (25) and (27) is an integer which means that whenever a zero is encountered that appears as a pole in the integrand, the resulting integral is

incremented by a factor of 2π by Cauchy's residue theorem. The contour integration in (25) and (27) is computed in a counter-clockwise manner, using an adaptive Gauss-Konrod quadrature (MATLAB's *quadgk* routine) [18]. The contour can be conveniently set up using the ‘waypoints’ parameter of the routine.

2.2 Locating the zeros

In this chapter, we use the derivative-free approach (27) to compute the number of zeros and further on. After predicting the number of zeros, the function f is then approximated by an associated *formal orthogonal polynomial* (FOP), \mathcal{P} of degree N , equal to the number of zeros. A necessary condition during approximation is that \mathcal{P} must have the same roots, z_k where $k = 1, 2, \dots, N$ as f . Furthermore, as stated earlier N must be less than N_r to avoid a too-high order polynomial for which the root-finding procedure would be very slow.

The polynomial \mathcal{P} can be represented in a Lagrange form:

$$\begin{aligned}\mathcal{P}_N(z) &= \prod_{k=1}^N (z - z_k) \\ &= z^N + \sigma_{N-1} z^{N-1} + \dots + \sigma_1 z + \sigma_0.\end{aligned}\tag{28}$$

To find the coefficients, σ_k we first define a symmetric bilinear operator similar to a dot product [19, 14],

$$\langle \phi, \psi \rangle = \frac{1}{2\pi j} \oint_{\Gamma} \phi(z) \psi(z) \frac{1}{f(z)} dz\tag{29}$$

where ϕ and ψ are polynomials of z . Next, we consider a set of integrals that are termed as the *Newton moments*,

$$s_p = \langle 1, z^p \rangle \frac{1}{2\pi j} \oint_{\Gamma} z^p \frac{1}{f(z)} dz.\tag{30}$$

which are then used as elements to construct Hankel matrices of size N ,

$$\mathbf{H} = \begin{bmatrix} s_1 & s_2 & \cdots & s_k \\ s_2 & s_3 & \cdots & s_{k+1} \\ \vdots & \vdots & \ddots & \vdots \\ s_k & s_{k+1} & \cdots & s_{2k} \end{bmatrix} \quad (31)$$

and

$$\mathbf{H}^< = \begin{bmatrix} s_0 & s_1 & \cdots & s_{k-1} \\ s_1 & s_2 & \cdots & s_k \\ \vdots & \vdots & \ddots & \vdots \\ s_{k-1} & s_k & \cdots & s_{2k-2} \end{bmatrix}, \quad (32)$$

in which the secondary diagonal terms are the same.

The polynomial \mathcal{P} in (28) is orthogonalized by enforcing the condition,

$$\langle z^k, \mathcal{P}_N(z) \rangle, \quad \text{where } k = 0, 1, \dots, N-1. \quad (33)$$

Because the operator $\langle \cdot, \cdot \rangle$ defined in (29) is not a dot product in true sense, that is why the term *formal* is included in the definition of the polynomial [19].

The polynomial in (28) can also be equivalently represented by a *companion* matrix, A as,

$$\mathbf{A} = \begin{bmatrix} 0 & 1 & 0 & \cdots & 0 \\ 0 & 0 & 1 & \cdots & 0 \\ \vdots & \vdots & \ddots & & \vdots \\ 0 & 0 & 0 & \cdots & 1 \\ -\sigma_0 & -\sigma_1 & -\sigma_1 & \cdots & \sigma_{N-1} \end{bmatrix}, \quad (34)$$

and $\mathcal{P}_n(z)$ can be obtained by setting its characteristic equation [20],

$$\det(A - \sigma_k I) = P(z), \quad (35)$$

where the eigenvalues are given by σ_k for the eigenvector z . The eigenvalue value problem of (35) can not be solved since the coefficients σ_k 's, where $k = 0, 1, 2, \dots, N-1$, are not

known yet. However, we can express σ_k 's in terms of the *Newton moments*, s_k 's through the *Newton identities*:

$$\begin{aligned} s_1 + \sigma_1 &= 0 \\ s_2 + s_1\sigma_1 + 2\sigma_2 &= 0 \\ &\vdots \\ s_N + s_{N-1}\sigma_1 + \dots + s_1\sigma_{N-1} + s_0\sigma_N &= 0. \end{aligned} \tag{36}$$

where we note that $s_0 = N$. We therefore, construct an equivalent eigenvalue problem using (31), (32) and (36) [14],

$$(\mathbf{H} - \lambda_k \mathbf{H}^{\leq}) \mathbf{z} = 0 \tag{37}$$

where the column vector \mathbf{z} is an eigenvector and λ_k 's are the eigenvalues of the matrix pencil $(\mathbf{H} - \mathbf{H}^{\leq})$, which correspond to the roots of $\mathcal{P}_n(z)$. In MATLAB, the routine *eig* is used to solve (37).

2.3 Refining the roots

The accuracy of the roots obtained from the eigenvalues, λ_k of (37) is not always high. However, λ_k 's is an excellent initial guess for any iterative root-search routine from the class of Householder's methods. We choose the *Newton* method [17] having quadratic convergence and the iteration formula:

$$x_{n+1} = x_n - \frac{f(x_n)}{f'(x_n)} \tag{38}$$

with $f'(x)$ is the first order derivative approximated by a finite difference formula (26). In general, the roots z_k 's are complex, therefore, the iteration (38) needs to be performed on both the real and imaginary parts simultaneously.

2.4 Avoiding singularities

As mentioned earlier, the argument principle method requires the function to be analytic without any singularities. In this chapter, we explicitly deal with the dispersion relation (23)

which is the denominator expression of the transmission line Green function. Therefore, branch point singularities only occur due to the presence of multivalued square roots that appear in the definition of the propagation constant, $k_{z,i}$ (20) with $i = 1, \dots, N$ and, N being the number of layers. The branch points exist provided the top and bottom layers are unbounded. The dispersion relation shows an even dependence on k_{zi} due to the layers that are bounded, hence they do not contribute any branch points [3, Section 5.3a]. In the worst case where the top and bottom layers are open and different from each other, two branch points exist in the complex plane that must be either removed or avoided in order to make the function analytic in the search region. Additionally, branch cuts emerge out of the branch points and there must not be any intersection with the contour of the search region.

In order to remove the branch point singularities, the complex z -plane is generally mapped to another plane ζ , by a transformation that unfolds the Riemann surface. For example, a trigonometric transformation such as [21, 22],

$$\begin{aligned} z &\mapsto \zeta \\ \zeta &= \cos(z), \end{aligned} \tag{39}$$

removes the branch point due to the multivalued propagation constant, k_{zi} , where $i = 1, N$ and makes the dispersion relation (23) analytic in the ζ -plane.

In this chapter, our goal is to find the surface waves from the dispersion relation. We only seek the *proper modes*, which are the roots of (23) that lie to the right of the branch point corresponding to $\max(k_{z1}, k_{zN})$. In order to satisfy the Sommerfeld radiation condition which requires all fields to decay to zero at infinity, the proper sheet of the Riemann surface of the square-root function needs to be selected. This is accomplished by enforcing that the imaginary part of k_{zi} that contributes a branch point, is negative everywhere.

$$\text{Im}(k_{zi}) < 0 \tag{40}$$

3 Results

3.1 MIM waveguide

We first compute the modes of a metal-insulator-metal (MIM) waveguide described in [23]. An air-filled region of thickness $d = \lambda/4$, where $\lambda = 1550\text{ nm}$ is sandwiched between two metal layers having permittivity ϵ_m . We first consider a lossless case in which ϵ_m has a value of -143.4967 , because of which the complex plane is essentially free from any branch-point singularities. For a TM case the dispersion relation is written as:

$$D = 1 - \left(\frac{Z_m - Z_2}{Z_m + Z_2} \right)^2 \times e^{(-2jk_z d)}, \quad (41)$$

where $Z_m = k_{zm}/(\omega\epsilon_m\epsilon_0)$ and $Z_2 = k_{z2}/\omega\epsilon_0$ are the modal impedances of the metal and air-filled layers respectively. The TM modes of (41) normalized to the free-space propagation constant are shown in Fig. 6a. The values of the roots obtained are then compared with the solutions discussed in [23], in which only the even modes were computed. However, as listed in Table. 1, we compute first nine even and odd modes.

Mode	This method (41)	Kocabas et. al. [23]
TM ₀	12.02 - j0.004432	12.03
TM ₁	11.85 - j0.008866	
TM ₂	11.34 - j0.008868	11.34
TM ₃	10.42 - j0.008867	
TM ₄	8.977 - j0.008867	8.981
TM ₅	6.681 - j0.008867	
TM ₆	0.8324 - j0.008867	0.7137
TM ₇	0. - j7.149	
TM ₈	0. - j10.53	0.008873 - j10.56

Table 1: TM modes of a lossless MIM waveguide

Next, we consider the lossy case where the permittivity of metal layers is $\epsilon_m = -143.5 + j9.517$ and the compared results are shown in Fig. 6a and listed in Table. 2.

Mode	This method (41)	Kocabas et. al. [23]
TM ₀	12.03 – j0.4001	12.03 – j0.3954
TM ₁	11.86 – j0.4100	
TM ₂	11.35 – j0.4283	11.35 – j0.4189
TM ₃	10.43 – j0.4651	
TM ₄	8.994 – j0.5380	8.996 – j0.5289
TM ₅	6.720 – j0.7170	
TM ₆	2.267 – j2.108	2.248 – j2.125
TM ₇	0.6612 – j7.188	
TM ₈	0.4504 – j10.54	0.4591 – j10.57

Table 2: TM modes of a lossy MIM waveguide

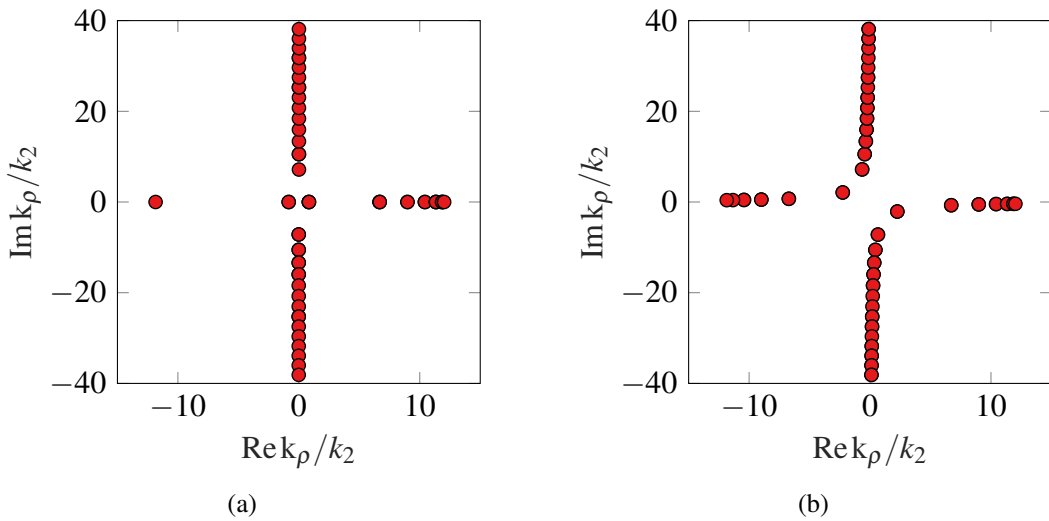


Figure 6: TM modes of a MIM waveguide (a) Lossless case, ($\epsilon_m = -143.5$) (b) Lossy case, ($\epsilon_m = -143.5 + j9.517$)

3.2 Embedded conductive sheets

Here we plot the dispersion curves of a 2DEG which is considered as a thin sheet embedded in a semiconductor heterostructure. We look at three types of structures,

1. Gated 2DEG
2. Ungated 2DEG
3. Backgated 2DEG,

that are classified, based on the presence of a perfectly conducting covering layer either at the top or bottom. The three types are shown in Fig. 7.

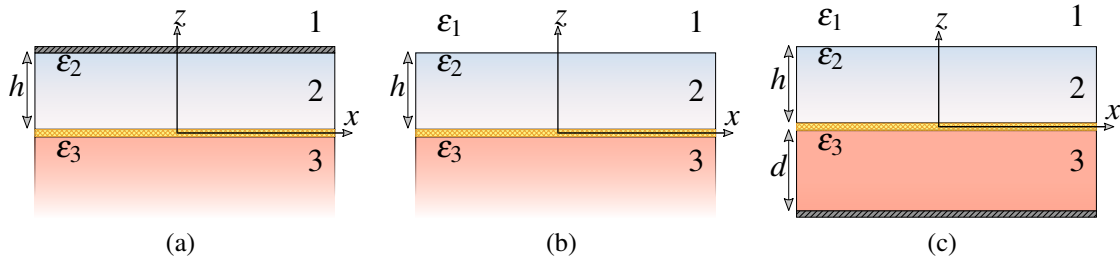


Figure 7: 2DEG embedded in a semiconductor heterostructure at $z = 0$ (a) Gated (b) Ungated (c) Backgated

We consider GaN/AlGaN (gallium nitride / aluminum gallium nitride) heterostructure with Al mole-fraction of $x = 0.2$. With respect to Fig. 7, Layer 1 is composed of GaN which is the substrate, considered open in the gated and ungated cases, while it has a thickness of $d = 50\text{ nm}$ in the backgated case. AlGaN forms the layer marked 2, and in all the three cases, a thickness, $h = 20\text{ nm}$ is assumed. The permittivity of both the layers is $\epsilon_r = 9.5$ owing to the small aluminum mole fraction [24]. The electron concentration of the 2DEG region is $N_s = 5 \times 10^{13} \text{ cm}^{-2}$ and scattering time τ of 114 ps corresponding to a temperature of 3 K is assumed. The surface conductivity is then computed using (22). When solving for the dispersion relation (23), we use the respective expressions listed in Table. 3 for each case.

Gated	Backgated	Ungated
$Y^\uparrow = -Y_2 \coth(k_{z2}h)$	$Y^\uparrow = Y_2 \frac{1-\Gamma^\uparrow}{1+\Gamma^\uparrow}$	$Y^\uparrow = Y_2 \frac{1-\Gamma^\uparrow}{1+\Gamma^\uparrow}$
	$\Gamma^\uparrow = \frac{Y_2-Y_1}{Y_2+Y_1} e^{-2jk_{z2}h}$	$\Gamma^\uparrow = \frac{Y_2-Y_1}{Y_2+Y_1} e^{-2jk_{z2}h}$
$Y^\downarrow = Y_3$	$Y^\downarrow = -Y_3 \coth(k_{z3}d)$	$Y^\downarrow = Y_3$

Table 3: Equivalent upward- and down-looking admittances

The dispersion curves for each structure type at varying temperatures and electron concentrations are plotted in Fig. 8.

To observe the effect of temperature, we now plot the dispersion curves at room temperature ($T = 295\text{ K}$) which corresponds to a scattering time, τ of 114 fs.

The conducting layer in the gated and back-gated cases depicts the gate terminal which is voltage biased in a normal transistor operation. By varying the voltage, we can subsequently modify the electron density in the 2DEG channel. In Figs. 10 and 11, the dispersion curves of gated and backgated structures are plotted for $N_s = 1 \times 10^{12}\text{ cm}^{-2}$ at 3 and 295 K respectively.

In the results shown, the lowest order TM_0 is plotted in all cases. By comparing the plots in Fig. 8 with the corresponding plots in Fig. 8, it is apparent that by increasing the temperature from liquid helium state to room temperature, loss expressed in terms of the imaginary part of the propagation constant is introduced. The imaginary part and the light line are enhanced for illustration.

The propagation constant belonging to the gated region exhibits a linear relationship [25, 26] as shown in Figs. 8a and 9a. Whereas a parabolic type dispersion curve is observed for the ungated region in Figs. 8c and 9c. For the backgated structure, the plot is initially linear for lower frequencies, followed by a parabolic region. The behavior is shown in Figs. 8b and 9b. Such a dispersion is generally attributed to surface plasmon polaritons existing at a dielectric-metal interface [27].

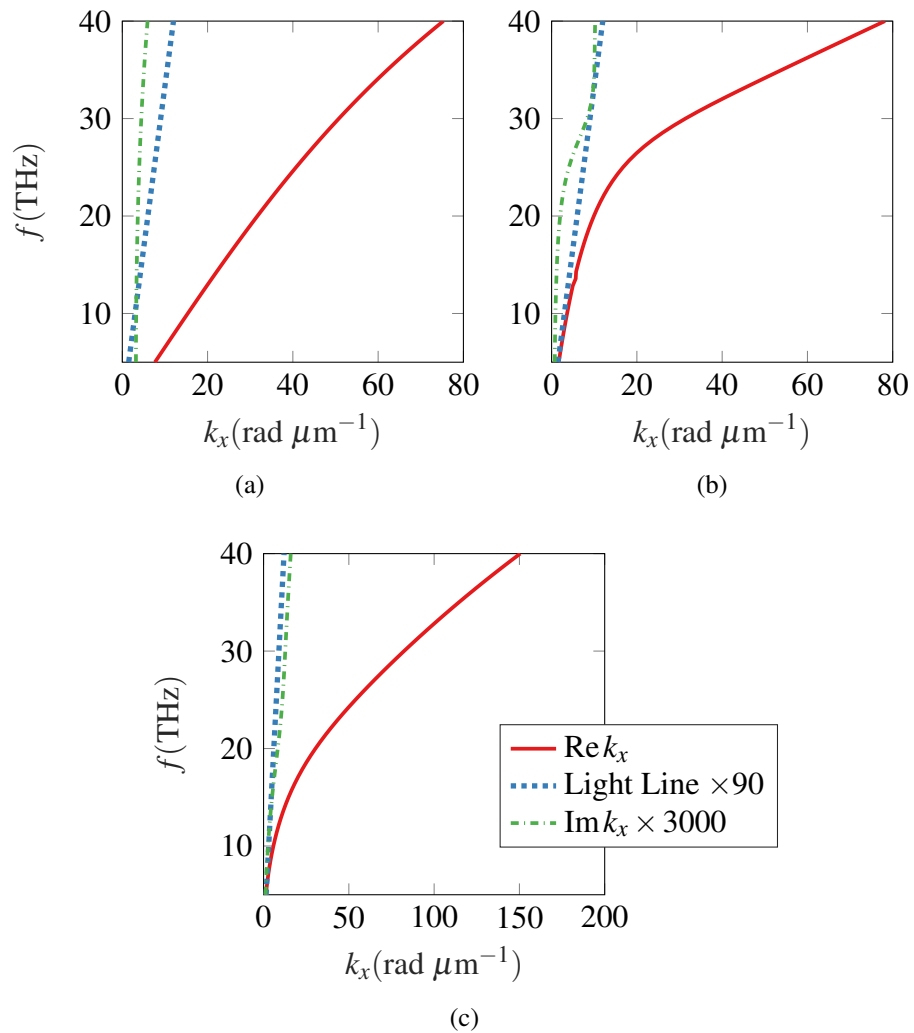


Figure 8: Dispersion Curves plotted for a GaN/AlGaN heterostructure with $N_s = 5 \times 10^{13} \text{ cm}^{-2}$ at 3 K (a) Gated (b) Backgated (c) Ungated

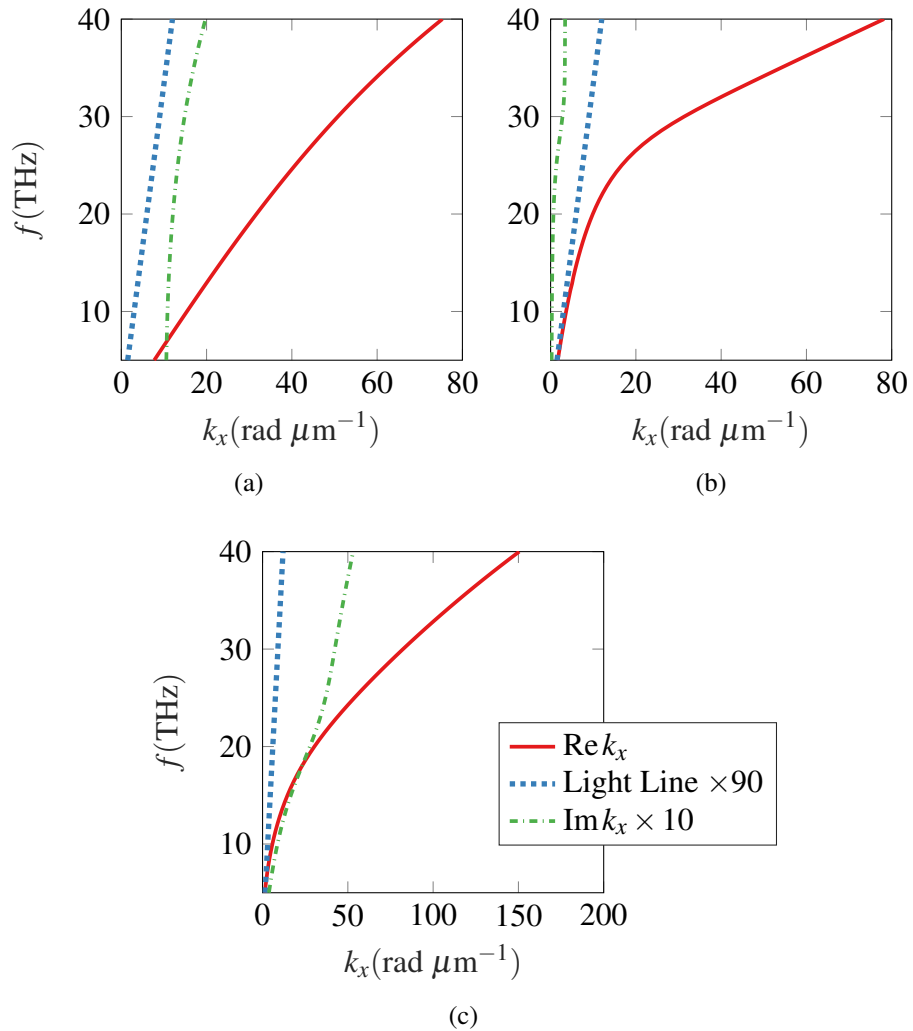


Figure 9: Dispersion Curves plotted for a GaN/AlGaN heterostructure with $N_s = 5 \times 10^{13} \text{ cm}^{-2}$ at 295 K (a) Gated (b) Backgated (c) Ungated

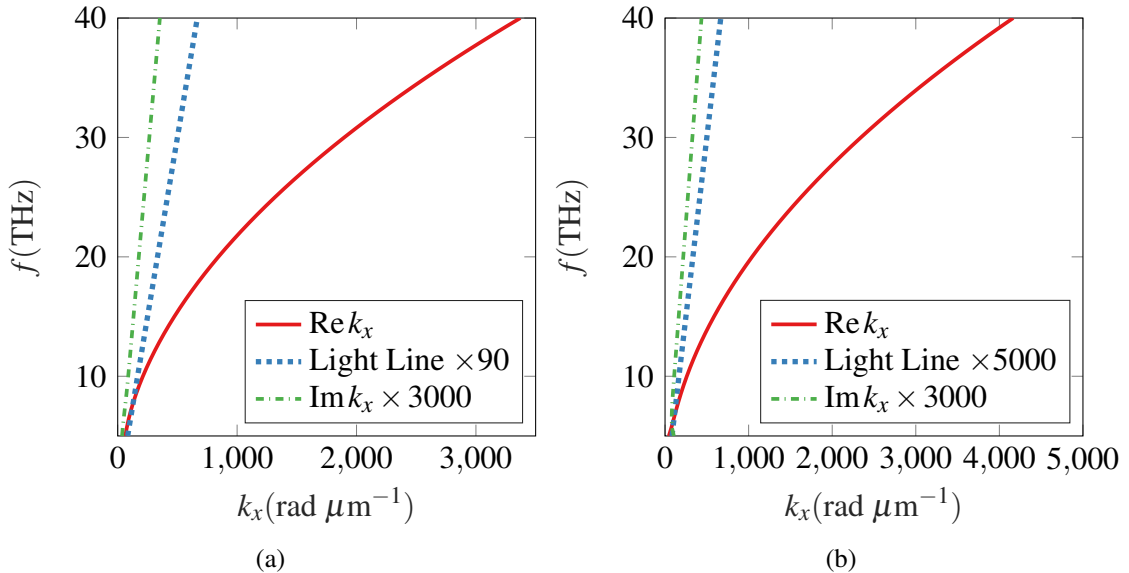


Figure 10: Dispersion Curves plotted for a GaN/AlGaN heterostructure with $N_s = 1 \times 10^{12} \text{ cm}^{-2}$ at 3 K (a) Gated (b) Backgated

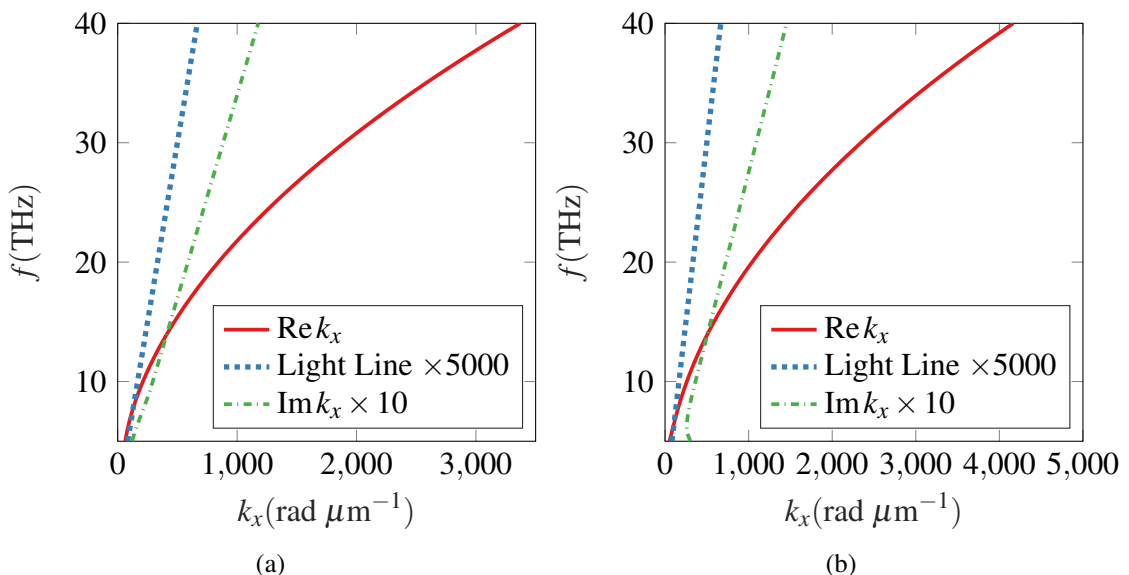


Figure 11: Dispersion Curves plotted for a GaN/AlGaN heterostructure with $N_s = 1 \times 10^{12} \text{ cm}^{-2}$ at 295 K (a) Gated (b) Backgated

Figures 10 and 11 show the plots of gated and backgated dispersion curves in which the 2DEG region is tuned to a lower electron concentration of $N_s = 1 \times 10^{12} \text{ cm}^{-2}$. Reduction of N_s by more than an order of magnitude results in a marked increase of the propagation constant [28].

4 Conclusion

In this chapter, the dispersion relation of various configurations of a GaN/AlGaN heterostructure is solved. The dispersion curves computed clearly show that the propagation constant in the 2DEG region, which is embedded in the multilayer, is much larger than free-space wavenumber. This translates to the ability to support subwavelength phenomenon. The effect of temperature on the associated loss is also observed.

References

- [1] K. Michalski and J. Mosig, “Multilayered media Green’s functions in integral equation formulations,” *IEEE Transactions on Antennas and Propagation*, vol. 45, no. 3, pp. 508–519, Mar. 1997.
- [2] K. A. Michalski, “Electromagnetic field computation in planar multilayers,” in *Encyclopedia of RF and Microwave Engineering*. John Wiley & Sons, Inc., Apr. 2005.
- [3] L. B. Felsen and N. Marcuvitz, *Radiation and Scattering of Waves (IEEE Press Series on Electromagnetic Wave Theory)*, ser. IEEE Press Series on Electromagnetic Wave Theory. Wiley-IEEE Press, 1994.
- [4] D. G. Fang, *Antenna Theory and Microstrip Antennas*. CRC PR INC, 2010.
- [5] T. Itoh, “Spectral domain imittance approach for dispersion characteristics of generalized printed transmission lines,” *IEEE Transactions on Microwave Theory and Techniques*, vol. 28, no. 7, pp. 733–736, Jul. 1980.
- [6] R. Kastner, E. Heyman, and A. Sabban, “Spectral domain iterative analysis of single- and double-layered microstrip antennas using the conjugate gradient algorithm,” *IEEE Transactions on Antennas and Propagation*, vol. 36, no. 9, pp. 1204–1212, 1988.
- [7] P. J. Burke, I. B. Spielman, J. P. Eisenstein, L. N. Pfeiffer, and K. W. West, “High frequency conductivity of the high-mobility two-dimensional electron gas,” *Applied Physics Letters*, vol. 76, no. 6, pp. 745–747, Feb. 2000.
- [8] J. S. Gómez-díaz and J. Perruisseau-carrier, “Propagation of hybrid transverse magnetic-transverse electric plasmons on magnetically biased graphene sheets,” *Journal of Applied Physics*, vol. 112, no. 12, p. 124906, Dec. 2012.
- [9] L. M. Delves and J. N. Lyness, “A numerical method for locating the zeros of an analytic function,” *Mathematics of Computation*, vol. 21, no. 100, pp. 543–543, 1967.

- [10] M. Carpentier and A. D. Santos, “Solution of equations involving analytic functions,” *Journal of Computational Physics*, vol. 45, no. 2, pp. 210–220, Feb. 1982.
- [11] L. Botten, M. Craig, and R. McPhedran, “Complex zeros of analytic functions,” *Computer Physics Communications*, vol. 29, no. 3, pp. 245–259, May 1983.
- [12] P. Kravanja, M. V. Barel, O. Ragos, M. Vrahatis, and F. Zafiropoulos, “ZEAL: A mathematical software package for computing zeros of analytic functions,” *Computer Physics Communications*, vol. 124, no. 2-3, pp. 212–232, feb 2000.
- [13] M. Dellnitz, O. Schütze, and Q. Zheng, “Locating all the zeros of an analytic function in one complex variable,” *Journal of Computational and Applied Mathematics*, vol. 138, no. 2, pp. 325–333, Jan. 2002.
- [14] C. Gillan, A. Schuchinsky, and I. Spence, “Computing zeros of analytic functions in the complex plane without using derivatives,” *Computer Physics Communications*, vol. 175, no. 4, pp. 304–313, Aug. 2006.
- [15] P. Y. Chen and Y. Sivan, “Robust Location of Optical Fiber Modes via the Argument Principle Method,” *Computer Physics Communications*, vol. 214, no. 2, pp. 105–116, May 2017.
- [16] S. G. Krantz, *The Argument Principle*. Boston, MA: Birkhäuser Boston, 1999, pp. 69–78.
- [17] W. H. Press, *Numerical Recipes*, 3rd ed. New York, NY, USA: Cambridge University Press, 2007.
- [18] L. Shampine, “Vectorized adaptive quadrature in MATLAB,” *Journal of Computational and Applied Mathematics*, vol. 211, no. 2, pp. 131–140, Feb. 2008.
- [19] P. Kravanja, T. Sakurai, and M. V. Barel, “On locating clusters of zeros of analytic functions,” *BIT Numerical Mathematics*, vol. 39, no. 4, pp. 646–682, 1999.

- [20] J. E. Gentle, “Computation of eigenvectors and eigenvalues and the singular value decomposition,” in *Statistics and Computing*. Springer New York, 1998, pp. 123–135.
- [21] K. A. Michalski, “Automatic, robust and efficient pole location for planar, uniaxial multilayers,” 2006.
- [22] A. G. Polimeridis, T. V. Yioultsis, and T. D. Tsiboukis, “An efficient pole extraction technique for the computation of Green’s functions in stratified media using a sine transformation,” *IEEE Transactions on Antennas and Propagation*, vol. 55, no. 1, pp. 227–229, Jan. 2007.
- [23] Ş. E. Kocababaş, G. Veronis, D. A. B. Miller, and S. Fan, “Modal analysis and coupling in metal-insulator-metal waveguides,” *Physical Review B*, vol. 79, no. 3, Jan. 2009.
- [24] A. V. Muravjov, D. B. Veksler, V. V. Popov, O. V. Polischuk, N. Pala, X. Hu, R. Gaska, H. Saxena, R. E. Peale, and M. S. Shur, “Temperature dependence of plasmonic terahertz absorption in grating-gate gallium-nitride transistor structures,” *Applied Physics Letters*, vol. 96, no. 4, p. 042105, Jan. 2010.
- [25] O. Sydoruk, J. B. Wu, A. Mayorov, C. D. Wood, D. K. Mistry, and J. E. Cunningham, “Terahertz plasmons in coupled two-dimensional semiconductor resonators,” *Physical Review B*, vol. 92, no. 19, Nov. 2015.
- [26] T. Ando, A. B. Fowler, and F. Stern, “Electronic properties of two-dimensional systems,” *Reviews of Modern Physics*, vol. 54, no. 2, pp. 437–672, Apr. 1982.
- [27] H. Yoon, K. Y. M. Yeung, P. Kim, and D. Ham, “Plasmonics with two-dimensional conductors,” *Philosophical Transactions of the Royal Society A: Mathematical, Physical and Engineering Sciences*, vol. 372, no. 2012, pp. 20130104–20130104, Feb. 2014.

- [28] O. Sydoruk, K. Choonee, and G. C. Dyer, “Transmission and reflection of terahertz plasmons in two-dimensional plasmonic devices,” *IEEE Transactions on Terahertz Science and Technology*, vol. 5, no. 3, pp. 486–496, May 2015.